JOURNAL OF APPLIED CRYSTALLOGRAPHY

Volume 51 (2018)

Supporting information for article:

Complete structural and strain analysis of single GaAs/(In,Ga)As/GaAs core–shell–shell nanowires by means of in-plane and out-of-plane X-ray nanodiffraction

Ali Al Hassan, Arman Davtyan, Hanno Küpers, Ryan B. Lewis, Danial Bahrami, Florian Bertram, Genziana Bussone, Carsten Richter, Lutz Geelhaar and Ulrich Pietsch

Supplementary Materials:

In addition to NW micro fields with different hole diameters and number densities (marked by red quadrats), NWs were grown in a single line with separation of 10 µm (Figure S1). This made it possible to access the side facets and edges of single NWs in the GID geometry. The NW orientation with respect to the incident beam direction is indicated, i.e. the incident beam is perpendicular to the NW side facet at $\varphi = 0^{o}$ and to the NW edge at $\varphi = 30^{o}$.

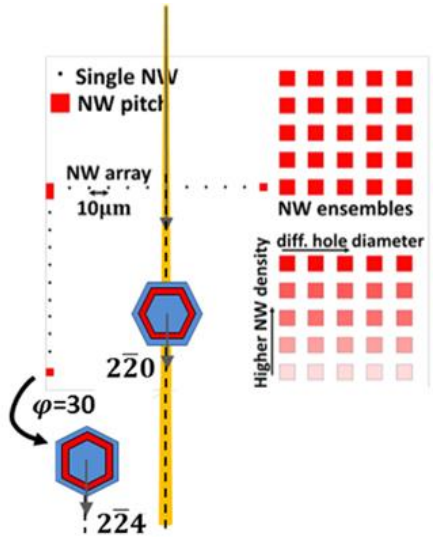

Figure S1: Top view of the lithography patterned sample mask along the NW orientation when the incident beam is perpendicular to the NW array. Single dots represent positions of single NWs.

Figure S2 shows the 3D RSM of the (111) Bragg reflection acquired at the mid-section of NW1 (Figure 2d). Apart from the NW Bragg peak (green and blue), the silicon crystal truncation rod (CTR) and contribution from parasitic objects are visible. The dominant features of the 3D RSM are the extended NW TRs along Q_x^{111} and Q_y^{111}. The thickness oscillations along the TRs encode the diameter of the entire NW.

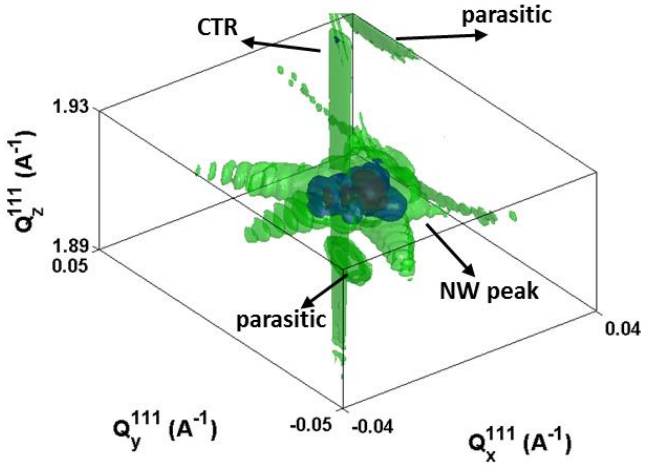

Figure S2: 3D RSM of the (111) Bragg reflection taken at the mid-section of NW1.

Figure S3 illustrates the XRD line profiles VLP1 and DLP1-2, displayed in Figure 4c, achieved by best fit of the FEM model in terms of shell thicknesses. The indium content was varied by ± 1% from the nominal value of 15%. Both structural parameters are listed on top of each subplot. An increase/decrease in the In content results in widening/shrinkage of the middle peak and an angular shift of the thickness oscillations. Nevertheless, both In contents of 14% and 15% show good agreement with the experimental data demonstrating the limit in the determination of In concentration at given experimental condition.

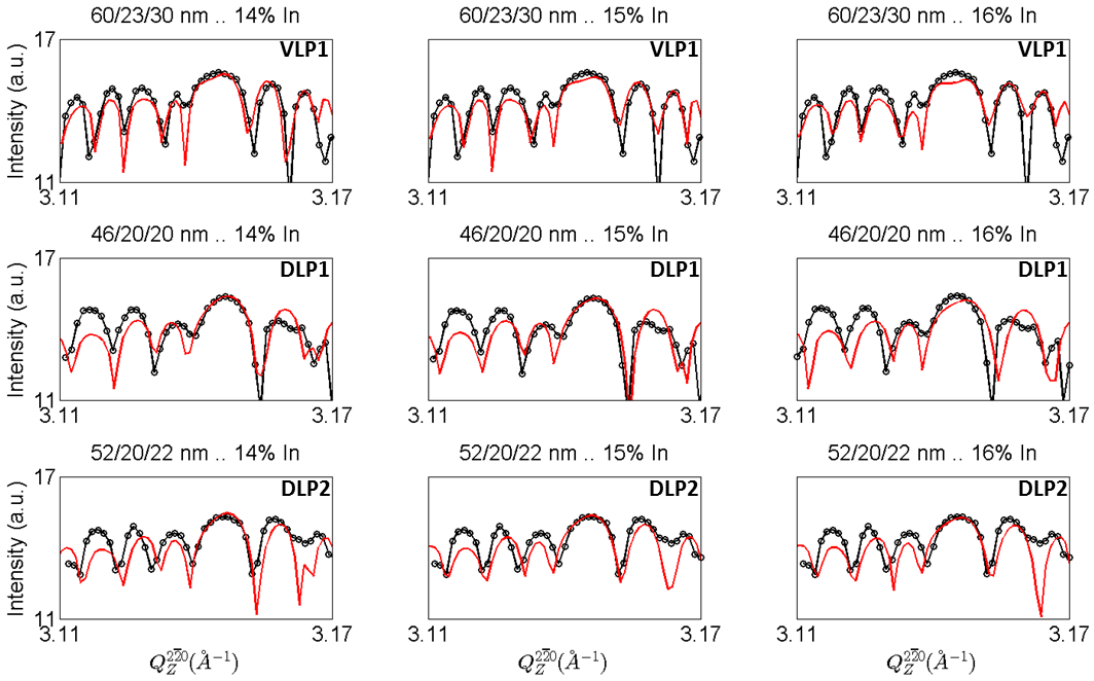

Figure S3: The three rows demonstrate FEM simulations of the three TRs labelled by VLP, DLP1 and DLP2 in the (2-20) RSM displayed in Figure 3a from top to bottom respectively. The three columns show FEM simulations for a variation of ± 1% with respect to the 15% nominal In content. The XRD data are labeled in black whereas the FEM simulations are labeled in red.

Figure S4 shows a selection of the GaAs/(InGa)As/GaAs NWHS FEM models used to fit VLP1 (Figure 4c). The best fit was achieved for a NWHS model with thicknesses of 60 nm/23 nm/30 nm (green dashed circle). To demonstrate the precision of the fitting process, the (In,Ga)As shell thickness was varied by 3 nm which resulted in a visible shift of the outer oscillations (blue dashed circle). Furthermore, FEM simulation using the nominal values of shell thicknesses shows bad agreement with the XRD line profile (orange dashed circle).

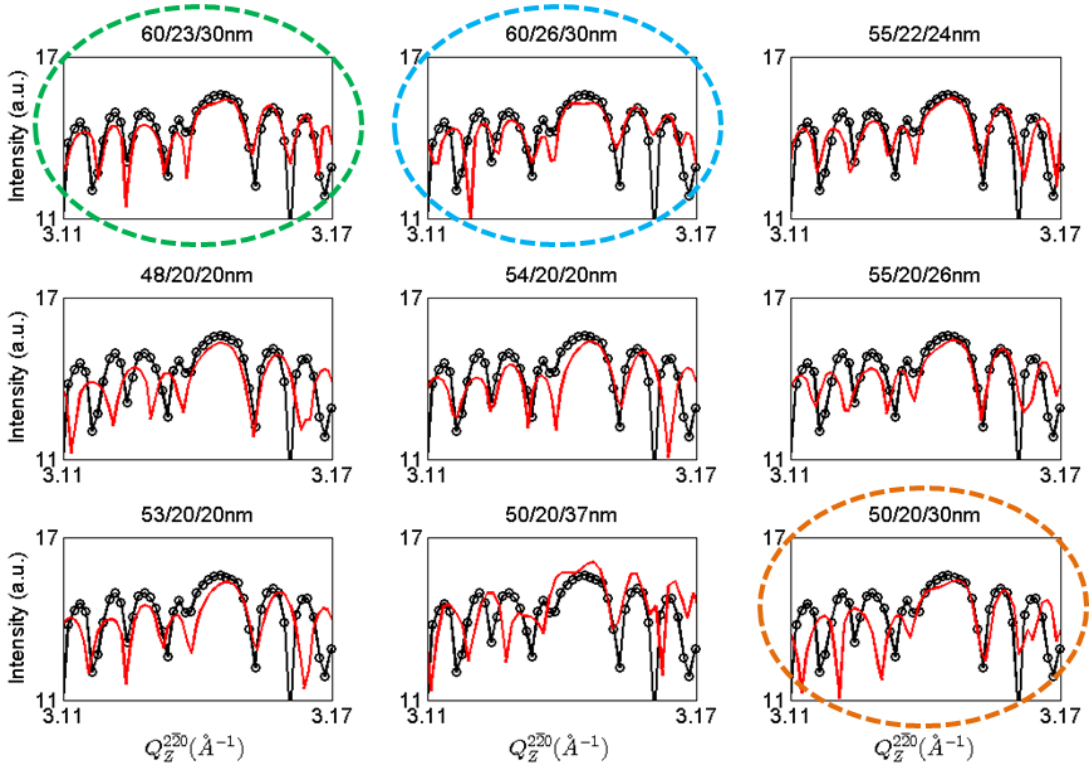

Figure S4: Portion of the GaAs/(In,Ga)As/GaAs combinations used in FEM to fit the VLP1 line profile from the 2-20 RSM plotted in Figure 4a. The XRD LP is colored in black whereas the FEM LP is colored in red. The FEM simulation of the 60 nm/23 nm/30 nm NW model, marked by a green circle, shows the best fit with respect to the experimental data. Varying the (In,Ga)As shell thickness by 3 nm, the FEM simulation does not longer fit the XRD LP precisely. This is marked by a blue dashed circle. FEM of single NW model with the nominal dimensions is marked in orange.

As mentioned in the manuscript, two approaches can be used to fit the line profiles extracted from XRD diffraction patterns. The RSMs of the (2-20) Bragg reflections of NW2 and NW4 are plotted in Figures S5a and S7a, respectively. The first approach is to use a distinct FEM NW model of perfect hexagonal shape to simulate each of the three TRs separately considering different shell thicknesses. The second approach is to simulate all TRs simultaneously using a unique NW model. The results of both approaches are demonstrated by blue and red lines in Figures S5 and S7 b-d, respectively. The fact that both approaches show good agreement with the experimental line profiles, demonstrates that the strains acting at the different pairs of opposite side facets are independent from each other. In contrast to NW2, NW4 displays a perfect hexagonal geometry.

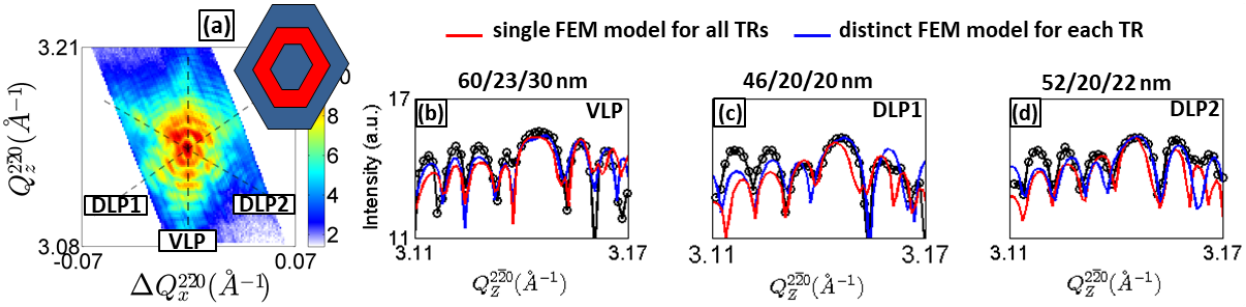

Figure S5: (a) RSM of the (2-20) Bragg reflection of the NW displayed in Figure 3a. On the top right corner, the predicted NW cross-section is plotted. (b-d) demonstrate FEM simulations and XRD LPs of VLP, DLP1 and DLP2. FEM simulations of distinct NW models are colored in blue whereas FEM LPs extracted from the NW model plotted in (a) are colored in red. XRD line profiles are colored in black.

Left panel of Figure S6 shows the 2D RSM of the (2-20) reflection acquired for NW4 whereas the right panel represents the diffraction pattern of the (22-4) Bragg reflection for a NW found outside the NW line shown in figure S1. Both RSMs show similar features compared to the findings of NW2 (Figures 3a and 3b).

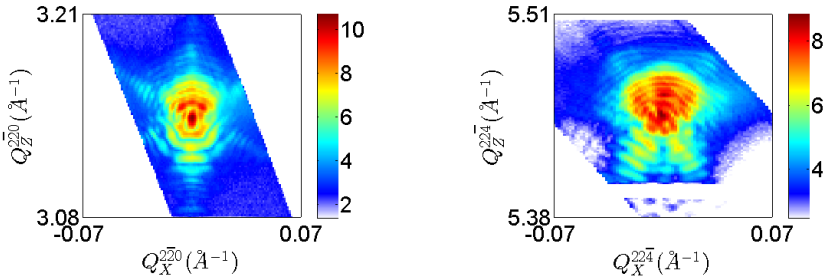

Figure S6: RSMs of the (2-20) and (22-4) Bragg reflections of two NWs from left to right, respectively.

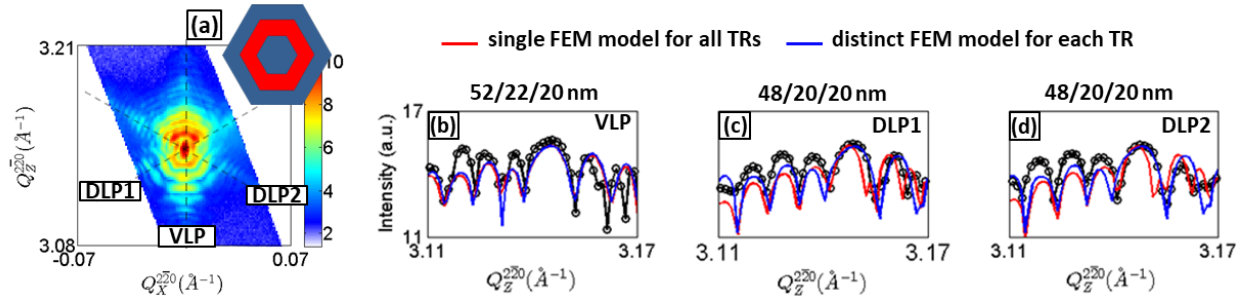

Figure S7: (a) RSM of the (2-20) Bragg reflection of NW4. On the top right corner, the predicted NW cross-section is plotted. (b-d) demonstrate FEM simulations and XRD LPs of VLP, DLP1 and DLP2. FEM simulations of distinct NW models are colored in blue whereas FEM LPs extracted from the NW model plotted in (a) are colored in red. XRD line profiles are colored in black.

Table 2: Core diameter and shell thicknesses, volume ratios and fitted In content are shown in the first five rows. The strain values estimated at the centers of the GaAs core, (In,Ga)As shell and GaAs cap along [111], [2-20] and [22-4] of NW4 and the strain gradient at each layer are shown below. Values inside absolute modulus represent the strain values at each interface of the corresponding shell (see Figure 5b). Both strain values and gradients have been extracted in the same manner as shown in Table 2 of the main part of the manuscript.

at center	GaAs core	(In,Ga)As	GaAs cap
VLP1 (nm)	52	22	20
DLP1 (nm)	48	20	20
DLP2 (nm)	48	20	20
In content	---	0.15 ± 0.01	---
Vol. fraction	0.14	0.34	0.52
$\boldsymbol{\varepsilon_c^{111}}$ (%)	+0.36	-1.41	+0.36
$\boldsymbol{\varepsilon_a^{2-20}}$ (%)	+0.08	+1.37	-0.27
$\boldsymbol{\varepsilon_b^{22-4}}$ (%)	+0.08	+1.18	-0.29
strain gradients	|(1) - (2)|	|(3) - (4)|	|(5) - (6)|
$\boldsymbol{\Delta\varepsilon_a^{2-20}}$ (%)	0.15 |0.08, -0.07|	0.25 |1.60, 1.35|	0.08 |-0.33, -0.25|
$\boldsymbol{\Delta\varepsilon_b^{22-4}}$ (%)	0.64 |0.08, 0.72|	1.86 |2.1, 0.24|	0.94 |-1, -0.06|

Figure S8 plots the RSM of the (22-4) Bragg reflection of NW5. Line profiles, named DLP3-4, indicated by oblique dashed black lines, were extracted along each TR to fit the experimental line profiles shown in Figures S8b and S8c. The best fits were obtained using NW models with thicknesses of 61/21/30 nm and 50/24/30 nm for DLP3 and DLP4, respectively. Based on the (22-4) Bragg reflection only, we are not able to fit a complete NW model.

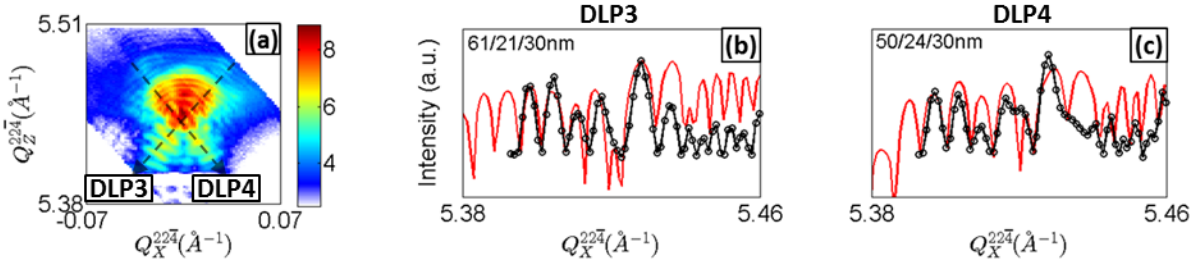

Figure S8: Panel (a) shows the 2D RSM of the 22-4 Bragg reflection from NW5. (b) and (c) FEM simulations and XRD LPs colored by red and black, respectively, and named DLP3 and DLP4 in (a). The structural parameters of the used FEM NW model are mentioned at the top left corners of subplots (b) and (c).